ON THE DEMISABILITY AND SURVIVABILITY OF MODERN SPACECRAFT

Mirko Trisolini[(1)], Hugh G. Lewis[(1)], Camilla Colombo[(2)]

[(1)] *Astronautics Research Group, University of Southampton, Southampton , SO17 1BJ, United Kingdom,* m.trisolini@soton.ac.uk, H.G.Lewis@soton.ac.uk

[(2)] *Department of Aerospace Science and Technology, Politecnico di Milano, Via La Masa 34, 20133, Milan, Italy,* camilla.colombo@polimi.it

ABSTRACT

In a period where the evolution of the space environment is causing increasing concerns for the future of space exploitation and sustainability, the design-for-demise philosophy has gained an increased interest. However, building a spacecraft such that most of it will demise through design-for-demise strategies may lead to designs that are more vulnerable to space debris impacts, thus compromising the reliability of the mission. Demisable designs will tend to favour lighter materials, thinner structures, and more exposed components, whereas survivability oriented designs will favour denser materials, thicker structures, and more protected components. Given the competing nature of the demisability and the survivability, we developed a multi-objective optimisation framework to evaluate the effect of preliminary design choices on the survivability and demisability of spacecraft components since the early stages of the mission design. Such method is applied to the representative test case of tank assemblies of Earth observation and remote sensing missions.

1 INTRODUCTION

In the past two decades, the attention on a more sustainable use of outer space has increased steadily. The major space-faring nations and international committees have proposed a series of debris mitigation measures [1, 2] to protect the space environment. Among these mitigation measures, the de-orbiting of spacecraft at the end of their operational life within 25 years is recommended in order to reduce the risk of on-orbit collisions. However, re-entering spacecraft can pose a risk to people and property on the ground. Consequently, it is necessary to assess the casualty risk related to the re-entry of a satellite, which needs to comply with the casualty limit of 10^{-4} if an uncontrolled re-entry strategy is to be adopted [3, 4]. A possible strategy to limit the ground casualty risk is to implement a design-for-demise strategy, where most (if not all) of the spacecraft will not survive the re-entry process. The implementation of design-for-demise strategies [5-7] may favour the selection of uncontrolled re-entry disposal options over controlled ones, leading to a simpler and cheaper alternative for the disposal of a satellite at the end of its operational life [6, 7]. However, a spacecraft designed to demise still has to survive the space environment for many years. As a large number of space debris and meteoroids populate the space around the Earth, a spacecraft can suffer impacts from these particles, which can damage the spacecraft or even cause the complete loss of the mission [8-10]. This means that the spacecraft and component design has also to take into account the survivability against debris impacts. The demisability and survivability of components and structures are both influenced by a set of common design choices, such as the material, the shape, the dimension, and position inside the spacecraft. It is important to consider such design choices and how they influence the mission's survivability and demisability from the early stages of the mission design process [7]. Taking into consideration these requirements at a later stage of the mission may cause an inadequate integration of these design solutions, leading to a delayed deployment of the mission and to an increased cost of the project. In general, the demisability and the survivability requirements have a competing nature. Consequently, a multi-objective optimisation framework has been developed, with the aim to find trade-off solutions for the preliminary design of satellite components. As the problem is nonlinear and involves the combination of continuous and discrete variables, classical derivative based approaches are unsuited and a genetic algorithm was selected instead. The genetic algorithm uses the previously described demise and survivability criteria as the fitness functions of the multi-objective algorithm.

Following these considerations, two models have been developed [11] to assess the demisability and the survivability of simplified spacecraft designs. The output from these models is used, in the form of fitness functions, in the multi-objective optimisation framework. Consequently, two fitness functions need to be defined to evaluate the level of survivability and

demisability. For the survivability, the probability of no-penetration (PNP) has been identified as the index to be used in the optimisation. For the demisability, three different indices are compared. A first index takes into account the amount of mass demised during the re-entry. The second index extends the first one, including the contribution of the demise altitude. The third index, additionally considers the effect of the casualty area of the surviving fragments.

A combined demisability-survivability analysis can be carried out on many different types of missions, provided that they can be disposed through atmospheric re-entry and they experience impacts from debris particles during their operational life. These characteristics are common to a variety of missions; however, it was decided to focus the current analysis on Earth observation and remote sensing missions. Many of these missions exploit sun-synchronous orbits due to their favourable characteristics, where a spacecraft passes over any given point of the Earth's surface at the same local solar time. Because of their appealing features, sun-synchronous orbits have high commercial value. Alongside their value from the commercial standpoint, they are also interesting for a combined survivability and demisability analysis. Sun-synchronous missions can in fact be disposed through atmospheric re-entry. They are also subject to very high debris fluxes [12] making them a perfect candidate for the purpose of this study.

The paper presents a test case, which considers the preliminary optimisation of propellant tanks in terms of material, geometry, location and number for representative sun-synchronous missions. The feasibility of the tank solutions is also evaluated comparing the stress on the walls of the tank with the ultimate strength admissible by the material used. The configuration of the external structure of the spacecraft instead is fixed. Tanks were selected because they are interesting for both the survivability and the demisability. They represent critical components in the demisability analysis as they usually survive the atmospheric re-entry. They are also components that need particular protection from the impact against space debris because such impacts can cause leaking or ruptures, which can compromise the mission success. Different configurations were analysed as a function of the characteristics of the tank assembly and of the mission itself, such as the mission duration and the mass of the spacecraft. The three different demisability fitness functions are also compared, highlighting the difference in the characteristics of the solutions provided, and discussing the quality of such solutions from a design-for-demise perspective. The results are presented in the form of Pareto fronts, which represent the different possible trade-off solutions for the tank assembly.

2 DEMISABILITY AND SURVIVABILITY MODELS

In order to carry out a combined demisability and survivability analysis of a spacecraft configuration it was necessary to develop two models [11, 13]. One model allows the analysis of the atmospheric re-entry of a simplified spacecraft configuration in order to evaluate its demisability. The other model carries out a debris impact analysis and returns the probability of no-penetration of the satellite as a measure of its survivability. As these two models need to be implemented into an optimisation framework, much effort was made to maintain a comparable level of detail and computational time between them.

2.1 Demisability model

The developed demisability model consists of an object-oriented code [14-16]. The main features of this type of code is the fast simulation of the re-entry of a spacecraft that is schematised using primitive shapes such as spheres, cubes, cylinders, and flat plates. These primitive shapes are used as a simplified representation of both the main spacecraft structure and internal components. The different parts of the spacecraft are defined in a hierarchical scheme with the main structure being the parent object and the internal components being the child objects that are contained inside the parent structure. For the simplified nature of the simulation carried out in object-oriented codes, the internal components do not experience any heat load until the main break-up event occurs. In the current model the break-up altitude is user-defined and is set to a default value of 78 km, which is the standard value used in most destructive re-entry software [17]. After the break-up occurs the child objects are separated from the main structure and their re-entry is simulated separately. The trajectory of the spacecraft is simulated with three degree-of-freedom ballistic dynamics. The computation of the attitude motion of the spacecraft is neglected and assumed to be random tumbling. Motion and shape averaged drag coefficients [18-20] are used for the aerodynamics of the spacecraft. The thermal load is computed using the Detra-Kemp-Riddel [20, 21] correlation and a set of motion and shape averaged shape factors [17, 18, 22, 23]. Standard models for the Earth's atmosphere and the gravitational field are used. Respectively, the 1976 U.S Standard Atmosphere [24], and the zonal harmonic gravity model up to degree four [25] are adopted. The material database used is the one available in the NASA Debris Assessment Software (DAS) [15].

The demise of components, i.e. the mass loss during the re-entry, is analysed using a lumped mass model where the temperature of the components remains uniform

over its entire volume. After the melting temperature is reached, the object starts to melt at a rate that is proportional to the heat load and the heat of fusion of the material.

2.2 Survivability model

The survivability model analyses the spacecraft configuration against the impact from untrackable space debris and meteoroids. For this procedure, the spacecraft was schematised with a panelised representation. To each panel is assigned a material and geometrical properties, as well as the type of shielding. The survivability model uses the same geometrical shapes of the demisability model in order to keep the two models comparable. Alongside the geometrical representation of the satellite, the characteristics of the space environment need to be known. This is achieved using the European Space Agency (ESA) software MASTER-2009 [26], which provides debris flux predictions for user defined target orbits. The 2D and 3D debris fluxes obtained from MASTER-2009 are used in conjunction with the geometrical characteristics of the spacecraft and the ballistic limit equations (BLE) to compute the penetration probability on each panel in which the structure is schematised using Poisson statistics [10, 27-29]. A more complete description of the procedure can be found in [11, 13].

A distinction needs to be made between the external structure of the spacecraft and the internal components. For the external structure, there is a direct impact with the space debris leading to the direct application of the procedure outlined before. On the other hand, when considering internal components, the debris clouds that develop inside the spacecraft after the impact need to be considered [8-10, 27]. These clouds can in fact hit and damage internal components. To consider how the impacts on the outer structure propagate into the inner components, two tools have been used: the Schafer-Ryan-Lambert ballistic limit equation (SRL-BLE) [10, 27], which can take into account impacts on multi-walled structures (up to three layers), and the concept of *vulnerable areas* [9]. The vulnerable area consists of an adjusted projection of an inner component onto the outer spacecraft structure. This area represents the portion of the external structure that, if impacted by a particle, could also lead to the impact of the inner component to which the relevant vulnerable area is associated. The SRL-BLE subsequently allows the direct calculation of the critical diameter associated with the inner components walls. In addition to the computation of the vulnerable areas and the critical diameters for the individual components, it is also necessary to consider the position of the components, and their mutual interaction inside the spacecraft. In fact, the position of the components inside the spacecraft produces mutual shielding of the components, reducing their vulnerability. The final step in the analysis is the computation of the vulnerability of each component inside the spacecraft and its external structure.

3 MISSION SCENARIOS

In order to demonstrate the simultaneous application of the demisability and the survivability models inside a multi-objective optimisation framework, the focus was on Earth observation and remote sensing missions [30, 31]. The reason behind this decision resides in the characteristics of their mission profiles, which usually exploit sun-synchronous orbits. In fact, such orbits are perfect candidates for a combined demisability-survivability analysis. As they are Low Earth Orbits (LEO), they allow the disposal of spacecraft through atmospheric re-entry. In addition, these orbits are highly polluted by space debris that can threaten the spacecraft reliability and survivability.

To estimate the overall size of the tank assembly it is necessary to compute the amount of propellant needed for the mission. As sun-synchronous orbits are influenced by atmospheric drag and by the non-uniformity of the Earth's gravitational field, they require regular orbit correction manoeuvres. They also need, as for most spacecraft, additional manoeuvres to correct orbit injection errors and to perform disposal manoeuvres. The computation of the different contributions to the delta-V budget is described in Section 3.1.

3.1 Delta-V budget computation

Orbit maintenance manoeuvres are used to maintain the sun-synchronism of the orbit and to control the ground track. To do so, the orbital height and inclination need to be maintained within admissible ranges. In LEO, atmospheric drag results in orbital decay, causing the semi-major axis and the orbit period to decrease. The reduction in the semi-major axis δa and in the orbital period $\delta\tau$ for one orbit can be computed as

$$\delta a = -2\pi\rho_{atm}\frac{SC_D}{m_s}a_0^{\,2} \tag{1}$$

$$\delta\tau = \frac{3\pi}{V_s}\delta a \tag{2}$$

where ρ_{atm} is the atmospheric density, S is the average cross section of the satellite, C_D is the drag coefficient, m_s is the mass of the satellite, a_0 is the nominal orbit semi-major axis, and V_s is the orbital velocity of the spacecraft. The changes in the orbital height and period lead to changes in the ground track. When the spacecraft's ground track reaches the prescribed

tolerance, a correction manoeuvre needs to be performed. First, the time difference from the nominal time at the equator passage Δt_0 needs to be computed:

$$\Delta t_0 = \frac{\Delta\lambda}{\omega_e} \tag{3}$$

where ω_e is the angular speed of the Earth and $\Delta\lambda$ is the longitude displacement at equator passage and can be expressed as:

$$\Delta\lambda = \frac{2E_0}{r_e} \tag{4}$$

r_e is the radius of the Earth, and E_0 is the imposed tolerance on the displacement from the nominal orbit ground track at the equator (equal to 0.7 km for this study). Using Eqs. 3 and 4 It is possible to compute the number of orbits after which the equator crossing displacement reaches the prescribed limit as follows:

$$k = \sqrt{\frac{2\Delta t_0}{\delta\tau}} \tag{5}$$

To control the ground track, the manoeuvre has to be executed every $2k$ orbits, leading to a variation in the orbit semi-major axis (Δa_{decay}) and orbital period (Δt_{decay}) of:

$$\begin{aligned} \Delta a_{decay} &= 2k\left|\delta a\right| \\ \Delta t_{decay} &= 2k\left|\delta\tau\right| \end{aligned} \tag{6}$$

Δt_{decay} is also the time between the necessary orbit correction manoeuvres. The correction manoeuvre can be computed with a Hohmann transfer as follows:

$$\Delta V_{decay,\,i} = \sqrt{\frac{\mu_e}{r_1}}\left(\sqrt{\frac{2r_2}{r_1+r_2}}-1\right)+\sqrt{\frac{\mu_e}{r_2}}\left(1-\sqrt{\frac{2r_1}{r_1+r_2}}\right) \tag{7}$$

where μ_e is the gravitational parameter of the Earth, $r_1 = a_0 - \Delta a_{decay}$ is the radius of the initial circular orbit, and $r_2 = a_0$ is the radius of the final orbit after the manoeuvre. The total ΔV_{decay} due to the orbital height correction manoeuvres for the entire mission lifetime is the sum of the contribution of Eq. 7 every Δt_{decay} so that:

$$\Delta V_{decay} = \left\lfloor \frac{t_m}{\Delta t_{decay}} \right\rfloor \Delta V_{decay,\,i} \tag{8}$$

where $\left\lfloor t_m / \Delta t_{decay} \right\rfloor$ represents the number of manoeuvres to be executed during the mission lifetime t_m. In addition, the orbit inclination needs to be controlled. In fact, the variation of the orbital inclination causes the drifting of the line of the nodes and affects ground track repetition and sun-synchronism. The total ΔV_{inc} needed to compensate for the inclination variation can be computed as

$$\Delta V_{inc} = 2\sin\left(\frac{\Delta i_{\text{sec}}}{2}\right)\cdot t_m \tag{9}$$

where Δi_{sec} is the secular variation of the inclination in one year that can be estimated to be equal to 0.05 deg/year, and t_m is the mission time in years. To compute the ΔV_{inj} needed to compensate for injection errors, we assume that the maximum errors in the orbital parameters after launch are:

$$\begin{aligned} \Delta a_{inj} &= \pm 35\ km \\ \Delta i_{inj} &= \pm 0.2\ \text{deg} \end{aligned} \tag{10}$$

The ΔV_{inj} due to the injection errors can then be computed using a Hohmann transfer with plane change where the initial and final orbits have a radius of $r_1 = a_0 - \Delta a_{inj}$ and $r_2 = a_0$ respectively, and the inclination change is equal to Δi_{inj}. Finally, the ΔV_{disp} to ensure the end-of-life disposal of the satellite can be estimated as follows. Assuming a spacecraft is able to naturally decay after 25 years from a 600 km altitude orbit, it is possible to approximate the disposal manoeuvre with a Hohmann transfer from the nominal orbit, to a 600 km orbit.

The sum of the previously computed ΔV values is the total ΔV_{tot} budget of a sun-synchronous mission, which depends on the nominal orbit of the spacecraft, the mission duration, and the characteristics of the spacecraft (mass, cross-section, drag coefficient).

$$\Delta V_{tot} = \Delta V_{decay} + \Delta V_{inc} + \Delta V_{inj} + \Delta V_{disp} \tag{11}$$

3.2 Storage volume computation

From the total ΔV required for the mission (Eq. 11), the amount of propellant required can be computed. For the purpose of this work, it is assumed that a monopropellant propulsion system using hydrazine as propellant is adequate for all the orbit correction manoeuvres described in Section 3.1. The specific impulse of hydrazine is 200 s. The propellant mass needed by the spacecraft during its entire lifetime can be computed using the Tsiolkowsky equation [30]:

$$m_p = m_{s,\,in}\left(1-e^{-\frac{\Delta V_{tot}}{g_0 Isp}}\right) \tag{12}$$

where m_p is the propellant mass needed to perform the total velocity change ΔV_{tot}, $m_{s,in}$ is the initial spacecraft mass, g_0 is the gravitational acceleration at sea level (equal to 9.81 m/s^2), and Isp is the specific impulse of the fuel used. Once the propellant mass is calculated, the total volume needed to store the propellant, considering also the filling factor of the tanks, can be

estimated as follows:

$$v_p = K1 \cdot \frac{m_p}{\rho_f} \tag{13}$$

where ρ_f is the density of hydrazine (equal to 1.02 g/cm^3), and $K1$ is a factor that takes into account the additional volume needed for the pressurant gas. For the entire article, $K1$ is assumed to have a value of 1.4 (average value from [32]), which is equivalent to a 60% filling factor. As an example, let us consider the MetOp mission [33]. MetOp is a sun-synchronous satellite with a mass of 4085 kg, and an average cross section S = 18 m^2. The operational orbit of the mission is 817 km in altitude with an inclination of 98.7 degrees. The mission design life is 5 years. Computing the mass of propellant with Eq. 12 with a specific impulse ranging between 220 s and 230 s, gives a propellant mass between 332 kg and 321 kg, which is very close to the actual mission value. Another example is the satellite Cryo-Sat2 [35], which is a 3 years mission with a satellite mass of 720 kg, an average cross section of 8.8 m^2, and an orbital altitude of 717 km. The resulting propellant mass is 43 kg, which is in good agreement with the value of 38 kg for the actual mission.

4 MULTI-OBJECTIVE OPTIMISATION

The developed multi-objective optimisation framework uses the demisability and the survivability models to find trade-off solutions in a context of a preliminary design of the spacecraft. In this way, a more integrated design can be achieved from the early stages of the mission design. Being able to discriminate between different alternatives for the design, taking into account the demisability and the survivability from the early stages of the mission design, is important. Being forced to change the mission design in later stages of the mission to comply with these requirements results in a longer development time and in a more expensive mission.

In its most general form, a multi-objective optimisation problem can be formulated as:

$$\begin{aligned} &\text{Min/Max } f_m(x), && m = 1,2,...,M; \\ &\text{Subject to } g_l(x) \le 0, && l = 1,2,...,\mathrm{L} \\ &h_b(x) = 0, && b = 1,2,...\mathrm{B}; \\ &\mathrm{x}_i^{(L)} \le x_i \le x_i^{(U)}, && i = 1,2,...,n. \end{aligned} \tag{14}$$

where x is a solution vector, f_m is the set of the m objective functions used, g and h are the constraints and $x^{(l)}$ and $x^{(U)}$ are the lower and upper limits of the search space. M is the total number of objective functions, and L and B are the total number of constraints, expresses respectively as inequalities and equalities.

In multi-objective optimisation, no single optimal solution exists that can minimise or maximise all the objective functions at the same time. Therefore, the concept of Pareto optimality is used. A Pareto optimal solution is a solution that cannot be improved in any of the objective functions without producing a degradation in at least one of the other objectives [36, 37].

There exists a large variety of optimisation strategies; however, for the purpose of this work and for the characteristics of the problem in question, genetic algorithms have been selected. The Python framework Distributed Evolutionary Algorithms in Python (DEAP) [38] was selected for the implementation of the presented multi-objective optimisation problem. Specifically, the selection strategy used is the Non-dominated Sorting Genetic Algorithm 2 (NSGAII) [37]. For the crossover mechanism, the Simulated Binary Bounded [39] operator was selected whereas for the mutation mechanism the Polynomial Bounded [40] operator was the choice.

Throughout this article, the input parameters to the genetic algorithm that define the characteristics of the evolution were fixed: the size of the population is 80 individuals, and the number of generations is 60. The crossover and mutation probability are 0.9 and 0.05 respectively.

4.1 Optimisation variables

The optimisation variables for the tank configuration taken into account in the present work are the material, thickness, shape, and the number of vessels in the assembly. The total tankage volume, which in turn influences the internal radius of the tanks, is determined using Eq. 13 and depends on the mission scenario.

For the material, the possible options are limited to three different materials commonly used in spacecraft —tank manufacturing. The possible materials are aluminium alloy Al-6061-T6, titanium alloy Ti-6Al-4V, and stainless steel A316. The characteristics of these materials are summarised in Table 1. ρ_{mat} is the material density, T_m is the melting temperature, C_m the specific heat, h_f the heat of fusion, ε the emissivity, σ_y the yield strength, σ_u the ultimate strength, and C the speed of sound in the material. Such material options have been considered also because of recent studies about design-for-demise solutions for tanks carried out within the ESA Clean Space framework, where a greater focus is dedicated to metallic options rather than composites solutions. The shape of the tanks can take two different geometries: a spherical tank or a right cylindrical tank, (represented in the optimisation using a binary value). These geometries were chosen because they are typical

of actual tank designs.

The number of tanks in which the propellant can be divided was varied from one to six units. It was assumed that six tanks would be a reasonable upper limit for the possible number of tanks to adopt.

Table 1: Properties of the materials used in the optimisation [41, 42].

	Al-6061-T6	A316	Ti-6Al-4V
ρ_{mat} (kg/m^3)	2713	8026.85	4437
T_m (K)	867	1644	1943
C_m (J/kg-K)	896	460.6	805.2
h_f (J/kg)	386116	286098	393559
ε	0.141	0.35	0.3
σ_y (MPa)	276	415	880
σ_u (MPa)	310	600	950
C (m/s)	5100	5790	4987

Lastly, the thickness of the tanks can be varied in the range 0.5 mm to 5 mm. This was considered a reasonable range for actual spacecraft tanks. Values smaller than 0.5 mm are considered too small, and more suitable for tank liners. Values larger than 5 mm were excluded because very thick metallic tanks would be too heavy. A summary of the variables of the optimisation with their respective values and range is provided in Table 2

Table 2: Summary of the optimisation variables with respective search spaces and types.

Variable	Range/Values	Variable type
Tank material	Al-6061-T6, Ti-6Al-4V, A316	Integer
Tank number	1 to 6	Integer
Tank thickness	0.0005 to 0.005 m	Real
Tank shape	Sphere, Cylinder	Integer

4.2 Constraint definition

As the analysis is considering possible configurations for a tank assembly, it is important to verify that such configurations are actually feasible. In fact, not all the combinations of dimension, thickness, shape, and material, can guarantee that the tanks will be able to withstand a standard operating pressure. To evaluate the feasibility of a solution, we compute the ultimate strength acting on the walls of a tank given its geometry, shape, and storage pressure. For cylindrical tanks, the ultimate strength can be expressed as follows:

$$\sigma_{u,wall} = \frac{\left(SF \cdot p \cdot r_{t,i}\right)}{t_s} \tag{15}$$

Whereas for spherical tanks the equivalent expression is

$$\sigma_{u,wall} = \frac{\left(SF \cdot p \cdot r_{t,i}\right)}{2t_s} \tag{16}$$

where $r_{t,i}$ is the internal radius of the tank, t_s its thickness, p the operating pressure, and SF a safety factor. For the remainder of this analysis, the operating pressure has been set equal to 4 MPa, which is a typical value for the storage of hydrazine in monopropellant propulsion systems [30]. Similarly, the value assumed for the safety factor is SF=1.5 that is a typical value for taking into account deviations from the mean operating pressure [32].

To assess the feasibility of a solution we simply verify that the ultimate strength on the walls of the tank is below the ultimate strength of the material of the tank :

$$\sigma_{u,wall} < \sigma_{u,material} \tag{17}$$

The implementation of the constraint inside the multi-objective optimisation algorithm is in the form of a *death penalty* [43], where unfeasible solutions are directly discarded.

4.3 Optimisation setup

Both the demisability and the survivability software require a simplified yet complete definition of the spacecraft configuration and of the mission characteristics in order to carry out their analyses. Therefore, alongside the optimisation variables (Section 4.1), other parameters need to be defined. First, it is necessary to define the mission scenario (Section 4.3.1) for both the demisability and the survivability. In the first case, this means defining the initial conditions of the atmospheric re-entry. In the second case, the operational orbit of the satellite and the mission duration need to be selected.

In the present work, the objective of the optimisation is to optimise tank configurations. Two aspects of the tank configuration that are not directly taken into account by the optimisation variables are the size and positions of the tanks (Section 4.3.3). It was decided to relate the size of the tanks, i.e. the radius, to the total volume required to store the propellant (Section 3.2) and to the number of tanks (see Eqs. 20 and 21) in order to have a realistic mission scenario. Delta-V budgets are in fact one of the main constraints on the mission design process and the amount of propellant, which is related to the size of the tanks, needs to be sufficient for the mission requirements.

Finally, both the demisability and the survivability analysis cannot be carried out without knowing the characteristics of the main spacecraft structure, i.e. the

overall size and mass of the satellite, the material, the thickness and the type of shielding (Section 4.3.2).

4.3.1 Mission scenarios

For the demisability simulation, the initial re-entry conditions are represented by the altitude, the flight path angle, the velocity, the longitude, the latitude, and the heading angle. Standard values for these parameters [22, 44] were selected and are presented in Table 3.

Table 3: Initial conditions for the re-entry simulations.

Parameter	Symbol	Value
Altitude	h_{in}	120 km
Flight path angle	γ_{in}	0 deg
Velocity	v_{in}	7.3 km/s
Longitude	λ_{in}	0 deg
Latitude	φ_{in}	0 deg
Heading	χ_{in}	-8 deg

For the survivability, the mission scenario is defined by the operational orbit of the satellite. As previously introduced (Section 3), we are considering sun-synchronous missions. As such, the orbit selected has an inclination of 98 degrees and an altitude of 800 km, which are typical values for sun-synchronous missions. In addition, four different mission durations were selected: 3, 5, 7, and 10 years.

4.3.2 Spacecraft external configuration

As the optimisation presented in the paper focuses on internal components (i.e. tanks), the external configuration of the spacecraft needs to be defined. It was decided to adopt a cubic shaped spacecraft in order to keep the analysis as general as possible. The dimensions of the cubic structure (i.e. its side length) can be computed tacking into account the mass of the satellite (m_s) and assuming an average density for the satellite (ρ_s) as follows [30].

$$L = \sqrt[3]{m_s / \rho_s} \tag{18}$$

It was assumed that the average density of the spacecraft is 100 kg/m^3, which is an average value that can be used in preliminary design computations [30].

Four classes of satellites were considered in the present analysis. The classes were defined according to the mass of the spacecraft: 500 kg, 1000 kg, 2000 kg, and 4000 kg options were considered. The classes and the corresponding spacecraft size, computed with Eq, 18 are summarised in Table 4. In addition to the size and mass of the spacecraft, the thickness and material of the external wall also need to be defined. For the purpose of this work, and in order to maintain the same conditions for all the simulations, it was decided to use a single wall configuration with a 3 mm wall thickness made of Aluminium alloy 6061-T6.

Table 4: Mission classes analysed with respective size of the satellite.

Class	Side length
500 kg	1.7 m
1000 kg	2.15 m
2000 kg	2.7 m
4000 kg	3.4 m

4.3.3 Tanks characteristics and positioning

Alongside the characteristics of the tank assembly defined through the optimisation variables (Section 4.1), it is necessary to define their location inside the spacecraft. For the purpose of this work, the location of the tank is not part of the optimisation process. It was thus decided to predefine the location as a function of the number of tank in the assembly. Because of the limitations on the position of the centre of mass of the satellite, it was decided to equally space the tanks around the centre of mass of the spacecraft. The centre of each tank is placed at the vertices of a regular polygon and the barycentre of the polygon coincides with the centre of the main spacecraft structure. For example, three tanks would be positioned as an equilateral triangle, four tanks as a square, and so on (Figure 2). As the tanks obviously cannot intersect each other, their mutual distance has to be bigger than twice their radius. With this consideration, the side length of the polygons can be computed as:

$$l = 2r_t \cdot K_2 \tag{19}$$

where r_t is the tank radius, and K_2 is a multiplicative factor to take into account the spacing between two tanks. For the analysis presented in this paper, *K2* has a value of 1.2.

As the total tankage volume is fixed by the mission characteristics and computed through Eq. 13, the external radius of the tank can be related to the number of tanks in the configuration. For spherical tanks, we have:

$$r_t = \sqrt[3]{\frac{3}{4\pi} \cdot \frac{v_p}{n_t}} + s_t \tag{20}$$

Whereas for right cylindrical tanks

$$r_t = \sqrt[3]{\frac{1}{2\pi} \cdot \frac{v_p}{n_t}} + s_t \tag{21}$$

Here, r_t is the outer radius of the tank, n_t is the number of tanks in the configuration, and s_t is the thickness of

the tank. An example of a configuration with four tanks is presented in Figure 1.

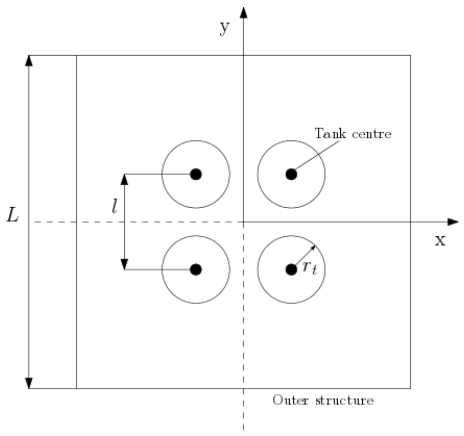

Figure 1: Example of a tank configuration with four tanks equally spaced with respect to the centre of mass of the spacecraft.

The possible tank configurations, ranging from one to six tanks, are schematically represented in Figure 2. The circles represent the positions of the centre of each tank. In each configuration, the tanks have the same shape, i.e. they are all spheres or all cylinders.

4.4 Fitness functions definition

The developed multi-objective optimisation framework uses the demisability and survivability models (Section 2) to evaluate the fitness of the generated solutions. A fitness function for both the demisability and the survivability needs to be defined.

4.4.1 Demisability fitness function

To evaluate the level of demisability of a certain configuration, three different possibilities for the fitness function have been considered in the following analysis. The first definition is the Liquid Mass Fraction (*LMF*), which is the fraction of the total re-entering mass melting during the atmospheric re-entry. The index is defined as follows:

$$LMF = \frac{\sum_{i=1}^{n_{comp}} LMF_i}{n_{comp}} \tag{22}$$

with

$$LMF_i = \begin{cases} 1 - \dfrac{m_{fin,i}}{m_{in,i}} & \text{if } e_{c,imp} > 15J \\ 1 & \text{if } e_{c,imp} \le 15J \end{cases} \tag{23}$$

Where LMF_i is the liquid mass fraction of the *i*-th component, n_{comp} is the number of component, $m_{fin,i}$ and $m_{in,i}$ are the final and initial mass of the *i*-th component respectively, and $e_{c,imp}$ is the impact energy of the *i*-th component. The index assumes that a component impacting the Earth with an energy below 15 J does not contribute to the casualty risk. As such, the *LMF* index is set to 1.0 when the impact energy is below 15 J

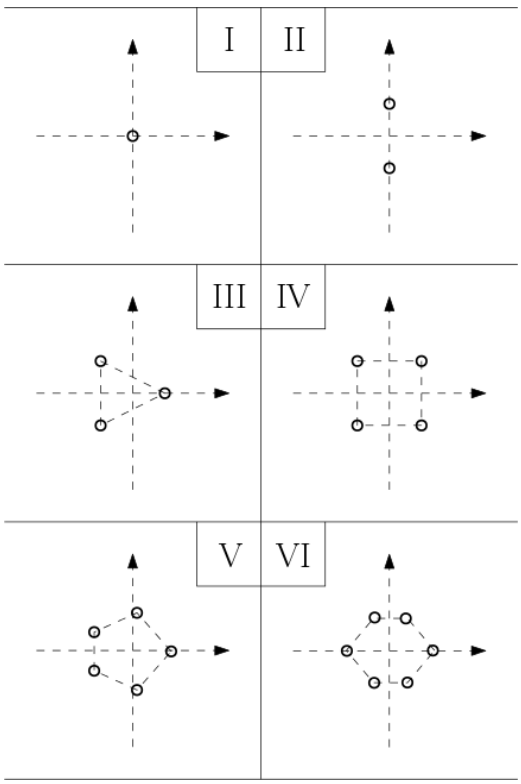

Figure 2: Possible configuration for the positioning of the spacecraft tanks.

The second proposed demisability fitness function, starts from the definition of Eq. 22, adding the contribution of the demise altitude (LMF_{DA}) of a component as follows:

$$LMF_{DA} = \frac{\sum_{i=1}^{n_{comp}} \left[LMF_i \cdot \left(1 + \dfrac{h_{demise,i}}{h_{in}} \right) \right]}{n_{comp}} \tag{24}$$

where LMF_i is defined as in Eq. 23, $h_{demise,i}$ is the demise altitude of the *i*-th component, and h_{in} is the initial altitude of the re-entry, which for internal components is equivalent to the break-up altitude. The decision to include a term that takes into account not just the amount of material demised through the re-entry but also the altitude at which the demise happens arises from a series of considerations. As destructive re-entry analyses rely on approximate methods and engineering correlations, it is important to consider safety margins when evaluating different solutions, especially in the early stages of the mission design. It is evident that, a

component with a higher demisability altitude would be a safer choice as it is more likely to demise even with varying entry conditions. The demise altitude is in fact an important output parameter in all the main destructive re-entry software, from NASA's DAS to ESA's DRAMA. The LMF_{DA} index favours demisable solutions, multiplying them by a factor that is proportional to the demise altitude. In addition, it allows the differentiation between different demisable solutions. With the first index (Eq. 22), all the solutions with a *LMF* index equal to 1.0 were equivalent, with this index they are discriminated by the actual demise altitude.

The third index considered, is based on the index of Eq. 24, with the additional consideration about the casualty area related to the surviving components:

$$LMF_{CA} = \frac{LMF_{DA}}{1 + \sum_{i=1}^{n_{comp}} A_{c,i}} \tag{25}$$

where $A_{c,i}$ is the casualty area of the *i*-th component. The casualty area is the sum of the cross section of all the components surviving the re-entry and impacting the ground. It is adopted in the computation of the casualty risk expectation. Adding this term to the demisability fitness functions allows two additional considerations to be linked to the fitness functions. First, it introduces, even if indirectly, a term that takes into account the casualty risk expectation related to a particular configuration. Second, it better discriminates between solutions with multiple components surviving the re-entry. In fact, increasing the number of components while reducing their dimensions is a strategy that allows the improvement of the demisability of a configuration. However, if these components do not demise, they represent a higher risk with respect to a single although larger component. The previous indices (Eqs. 22 and 24), as they perform an average over the surviving components, cannot properly distinguish between solutions with a different number of surviving objects. Adding the contribution of the casualty area adds this feature to the demisability fitness function.

4.4.2 Survivability fitness function

To evaluate the level of survivability, the probability of no-penetration (*PNP*) was selected as the fitness function. The probability of no-penetration represents the chance that a specific spacecraft configuration is not penetrated by space debris during its mission lifetime. In this case, the penetration of a particle is assumed to produce enough damage to the components to seriously damage them so that the *PNP* can be considered a sufficient parameter to evaluate the survivability of a satellite configuration. The overall probability of no-penetration of a spacecraft configuration is computed as follows:

$$PNP = 1 - \sum_{j=1}^{N} P_{p,\mathrm{j}} \tag{26}$$

where $P_{p,j}$ is the penetration probability of the *j*-th component.

5 RESULTS AND DISCUSSION

As previously introduced, the developed multi-objective optimisation framework has been applied to a test case, considering the optimisation of spacecraft tanks for a simplified spacecraft configuration. The problem in exam of considering a combined demisability-survivability analysis is very much mission dependent. In fact, the mission time influences the amount of debris impacts on the satellite and consequently its probability of no-penetration. The size and mass of the spacecraft and its components strongly influence the demisability. The geometry, the quantity, and the material of the components very much affect both the demisability and the survivability. For these reasons, it was decided to perform the optimisation for different spacecraft masses and mission lifetimes. In addition, the three different demisability fitness functions have been compared.

Starting with the index of Eq. 22, the general characteristics of the Pareto front are analysed. Figure 3 represents the Pareto fronts for a 2000 kg spacecraft with a mission lifetime of 10 years with a maximum allowed number of tanks equal to three. The mission scenario is the one described in Section 4.3.1. In the Pareto front, the different solutions are distinguished as follows: the colours indicate the three materials, the marker shape indicates the configuration of the tank assembly, i.e. the number of tanks. The difference between cylindrical and spherical tanks is highlighted by starring the spherical solutions, while leaving unmarked the cylindrical ones.

From the graph of Figure 3 it is possible to observe a number of features of the optimisation results. First, the expected competing behaviour between the demisability and the survivability is clearly represented by the shape of the Pareto front with high demisability solutions having a relative low probability of no-penetration and vice versa. Second, the ranges for the two indices are considerably different. This is indeed expected, given the very different domains described by the two models. In particular, the survivability has a naturally narrow range of values, considering that a PNP index of 95%-98% is typical for many missions (obtained as the sum of the contribution of every component in the spacecraft). As such, even small variations at component level can be significant, especially when these components are critical to the mission success. For example, the overall probability of no-penetration for the MetOp SVM satellite evaluated with the software

SHIELD [9], is 97.26%, and the tank assembly (four tanks in total) probability of no-penetration is 99.78%, which is comparable with the value obtained in the presented optimisation.

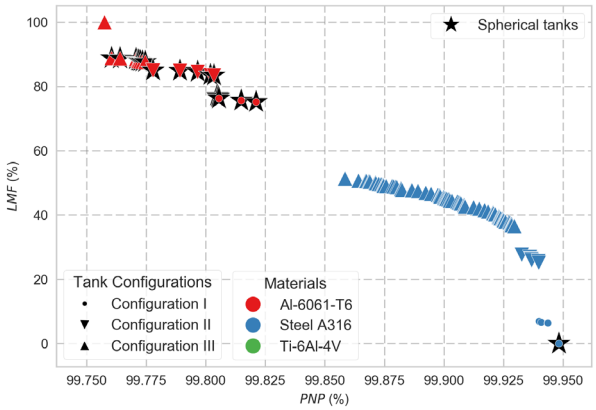

Figure 3: Pareto front for a 2000 kg spacecraft for a 10 years mission lifetime and a maximum allowed number of tanks equal to 3.

Looking more closely at the solutions obtained by the optimiser, it is first recognisable that there is a separation between the three materials considered. The aluminium solutions are identified by the greatest demisability and lowest survivability, whereas the stainless steel solutions with higher survivability and lower demisability. Only one titanium alloy solution has been identified and is the one with the greatest survivability. In fact, titanium solutions are always dominated by other solutions in terms of the demisability, given their high temperature resistance. However, among the low demisability solutions, they are more resistant to debris impacts than the stainless steel equivalents. Another recognisable trend is the presence in both the aluminium and stainless steel groups of solutions corresponding to configurations with one, two, and three tanks. As the number of tanks increases, the demisability improves and the survivability deteriorates. However, the reduction of the survivability index because of the increased number of vessels does not prevent these solutions from dominating configurations with a lower amount of tanks. From this behaviour, it can be inferred that adopting a design strategy that substitutes physically large components with a higher number of smaller components has a greater impact on the demisability of a configuration with respect to the survivability. Another evident feature of the Pareto front is the distribution of the spherical tank solutions. All aluminium alloy solutions except for one are spherical, whereas no stainless steel solution is. The important difference between spherical and cylindrical tanks is their ultimate strength, as spherical solutions have twice the ultimate strength of cylindrical tanks with the same radius and thickness. As the aluminium alloy has a lower ultimate strength than the stainless steel, the shape of the vessel has a considerable impact on the optimisation output, as many cylindrical solutions results are unfeasible. However, it is possible to observe that the solution having a 100% LMF index actually has cylindrical tanks because they guarantee a better demisability. On the other hand, for the stainless steel case, both the spherical and the cylindrical solutions are sufficiently resistant. Therefore, the optimiser favours cylindrical solutions, as they are more demisable than equivalent spherical solutions.

All the solutions presented in the Pareto front of Figure 3 are viable design solutions. As such, they can all be considered in a preliminary design phase. Then according to the mission requirements and other mission constraints, a more detailed analysis will follow for some of them. For example, the optimiser has identified one fully demisable solution, which consists of three cylindrical aluminium tanks. However, other high demisability solutions may be worth further investigation, because they could be demisable when a more refined analysis is carried out

5.1 Varying the maximum allowed number of tanks

Varying the number of vessels in which to split the propellant is an effective strategy to improve the demisability. A larger number of smaller tanks are in fact more easily demisable than a single very large tank. However, increasing the number of components also increases the exposure of the spacecraft to space damaging debris impacts. Figure 4 and Figure 5 represent the Pareto fronts for the same mission profile of Figure 3 with the only difference being the maximum number of tanks allowed by the optimiser. In these cases, this amount was set to two and six respectively.

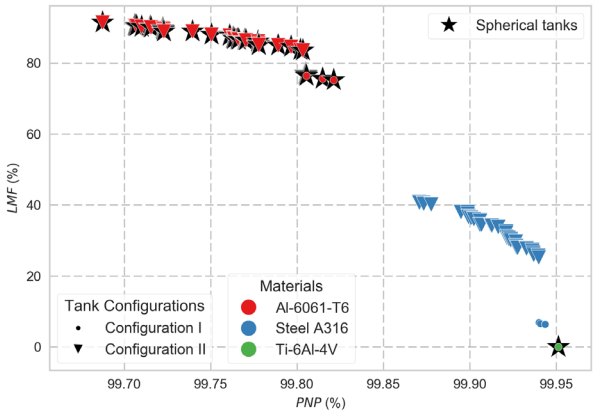

Figure 4: Pareto front for a 2000 kg spacecraft for a 10 years mission lifetime and a maximum allowed number of tanks equal to 2.

Examining both graphs, it can be noticed that it is the tendency of the optimiser to select solutions with the maximum possible number of tanks. Another observable trend is the increasing ratio between stainless steel and aluminium alloy solutions as the number of tanks allowed increases. As stainless steel solutions become more demisable, given the possibility of using smaller vessels, they tend to dominate more aluminium solutions thanks to their better performances with respect to the survivability. Another interesting aspect can be observed in Figure 4, where no solution is fully demisable. Even the aluminium alloy cases are not completely demisable as the minimum thickness required to be feasible is not small enough to guarantee the demise. This underlines the importance, from a design-for-demise standpoint, of the subdivision of large components into smaller parts. This could lead to a requirement definition for spacecraft tanks, even on medium sized satellites.

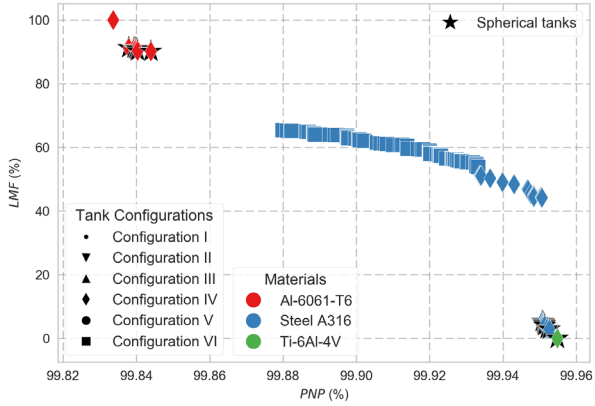

Figure 5: Pareto front for a 2000 kg spacecraft for a 10 years mission lifetime and a maximum allowed number of tanks equal to 6.

5.2 Varying the mission lifetime

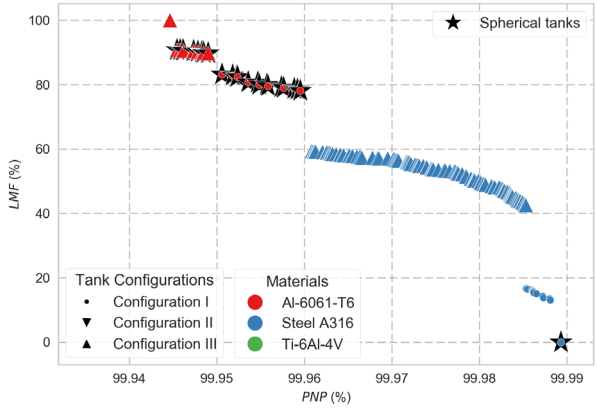

Figure 6: Pareto front for a 2000 kg spacecraft for a 3 years mission lifetime and a maximum allowed number of tanks equal to 3.

As shown in Figure 6, varying the mission lifetime mainly influences the extent of the *PNP* index range. As expected, lower mission lifetimes generate narrower ranges, and in particular, they reduce the lower limit for the probability of no-penetration. This is an expected yet important behaviour. In fact, it is possible that, for some mission profiles, implementing design-for-demise solutions do not result in a significant deterioration of the survivability of the satellite.

5.3 Varying the mission mass

Another important aspect discriminating the mission typology is the mission mass. In fact, the mission mass can be related to the size of the satellite and to the propellant requirements of the mission (thus changing the size of the tanks). Figure 7 and Figure 8 show the Pareto front for the same mission scenario of Figure 3 but for a 1000 kg and a 4000 kg mission respectively. A clear trend is the increase in the number of aluminium alloy solutions as the mass of the mission increases.

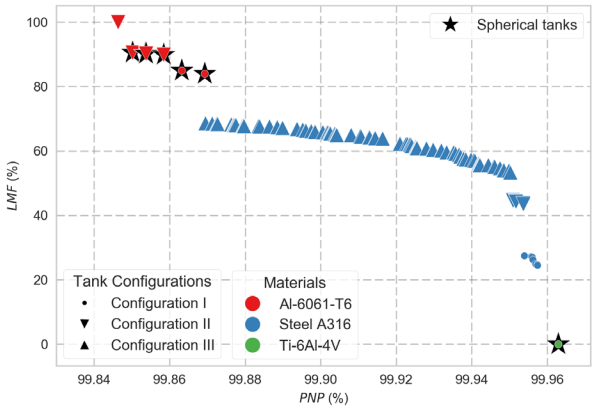

Figure 7: Pareto front for a 1000 kg spacecraft for a 10 years mission lifetime and a maximum allowed number of tanks equal to 3.

Missions that are more massive requires larger tanks, therefore more aluminium solutions start to dominate stainless steel solutions given their higher demisability. Additionally, the difference in the demisability between the aluminium and the stainless steel solutions increases as the mass increases, more clearly discriminating between solution with high demisability and with high survivability. This indicates that, when considering tank assemblies, an increasing mass amplifies the dichotomy between demisable and survivable solutions, giving more importance also to other design parameters such as the external shielding of the satellite, which is not taken into account in this study. This is even more important when other types of components are considered in a more complete architecture of the spacecraft. In addition, it is possible to observe from Figure 8 that no solution is fully demisable. Therefore, a 3-tank

configuration is not enough for the 4000 kg satellite analysed to obtain fully demisable solutions. This highlights how the design-for-demise solutions are coupled not just with the mission scenario but also with the main characteristics of the spacecraft.

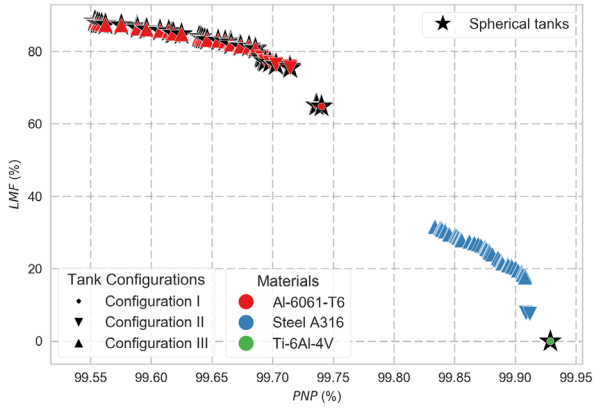

Figure 8: Pareto front for a 4000 kg spacecraft for a 10 years mission lifetime and a maximum allowed number of tanks equal to 3.

5.4 Comparison of demisability indices

As previously introduced, three different demisability fitness functions have been proposed. The comparison between the three indices for the same spacecraft and mission scenario of Figure 3 is presented in Figure 9. The first recognisable difference between the three plots is the range of the *PNP* index, with clearly a larger range for the second and third indices. The maximum value of the probability of no-penetration remained unchanged, although the lower limit shifted towards lower values as new solutions are found to be changing the index. The reason for such behaviour is the higher differentiation of demisable solutions that is introduced with the indices of Eqs. 24 and 25. In fact, when using the first index (Eq. 22), all the demisable solutions, i.e. the solutions with an impact energy lower than the 15 J threshold, are equivalent, with an index value of 1.0. Instead, the other two indices differentiate between these solutions by taking into account the demise altitude. In this way, not all the demisable solutions are equivalent and a greater range of possible designs can be taken into account.

For what concerns the first two indices, the two Pareto fronts results are equivalent, with the same distribution of solutions, except for the high demisability area, showing the behaviour previously described. On the other hand, the third index departs more from the other two. In fact, even if it exhibits the same behaviour of the second index for high demisability solutions, it clearly has a different behaviour for non-demisable solutions. A first feature that can be observed is a downshifting of all the non-demisable solutions towards lower values of the index. This is a direct consequence of considering the contribution of the casualty area.

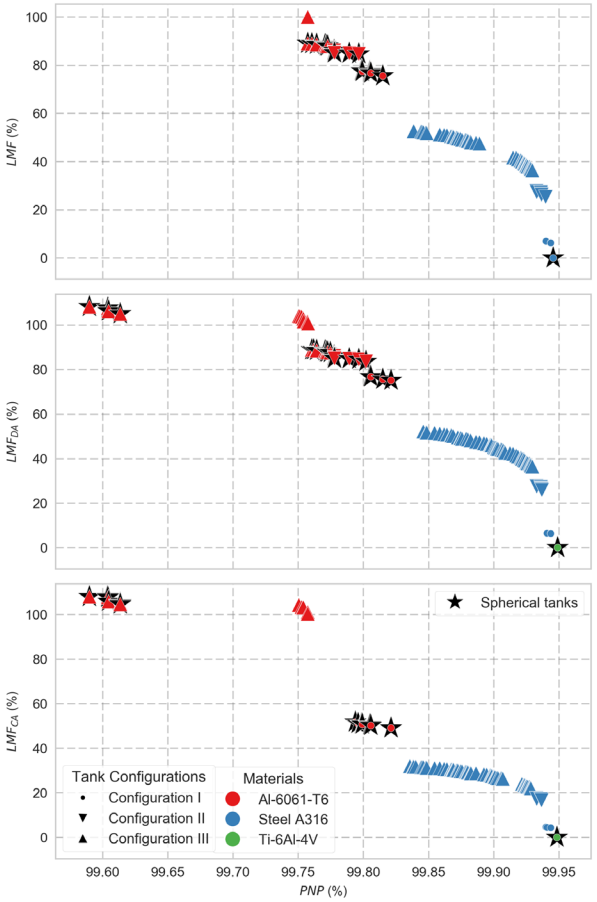

Figure 9: Comparison between the three proposed demisability indices for a 2000 kg spacecraft for a 10 years mission lifetime and a maximum allowed number of tanks equal to 3.

In fact, only a component surviving the re-entry, contributes to the casualty area. As such, all surviving configuration will be penalised by a value that is proportional to the casualty area associated to the solutions. Another feature introduced with the index of Eq. 25 is a difference in the configuration selected by the optimiser for non-demisable solutions. Whereas for the first two indices the optimisation always produces a greater number of solutions with the highest allowed number of tanks in the assembly, for the third index, this is not the case, at least for the aluminium solutions. In fact, it is possible to observe that among the surviving aluminium tanks, configurations with one tank are always preferred. This is a desired behaviour for a demisability index. Has we have seen, using a larger number of smaller component is a useful and effective design-for-demise strategy in order to achieve the demisability of a configuration. However, when such a

configuration does not achieve the demisability, it is actually more dangerous as it produced a greater number of fragments reaching the ground. However, this is not observed for the stainless steel tanks. This means that the contribution of the demised mass outweighs the one of the casualty area even for configurations with larger number of tanks, for the adopted index definition. An important aspect is also represented by the cylindrical demisable solutions with a *PNP* of about 99.75%. With the newly introduced index, these solutions clearly stand out and separate themselves from the more regular trend of the above Pareto fronts. This identifies these solutions as very appealing, given their high demisability and average survivability. The separation of these solutions from the rest of the Pareto front is clearly introduced by the index of Eq. 25, given its penalisation of non-demisable solutions.

6 CONCLUSIONS

The development of an optimisation framework allowing the trade-off analysis between the demisability and the survivability of preliminary design solutions has been presented. Given the characteristics of the demisability and survivability models implemented, the optimisation is able to consider simplified configurations (typical of preliminary design assessments), schematised with a set of simplified geometries, representing spacecraft components, and grouped into a parent-child hierarchy. Each representative component is defined through its geometry, material, and location inside the spacecraft. The external structure of the spacecraft also takes into account the type of shielding adopted. All of these features can be considered in the models. However, to demonstrate the features of the framework, the application to sun-synchronous missions and to a specific type of component, i.e. tanks, has been considered. In fact, the case of tank assemblies was considered of importance, given the high interest in the design-for-demise field for such components. The analysis was also extended to consider different types of spacecraft classes based on their mass, and mission lifetimes. In addition, the influence of the choice of the demisabilty fitness function has been analysed, studying the effects of three different fitness functions for the evaluation of the demisability.

The optimisation of the tank assembly takes into account several aspects of their design: the material, the thickness, the number of tanks, and the shape. In addition, the dimensions of the tanks are linked to the actual characteristics of the mission, computing the amount of propellant needed during the mission lifetime. In addition, the constraint on the feasibility of the solutions given the allowed maximum storage pressure of a certain tank design is also addressed. Considering all these aspect, a number of interesting observations could be made from the Pareto fronts obtained through the optimisation. First, it is important to observe that the optimiser was able to find trade-off solutions, actually confirming the competing behaviour existing between the demisability and the survivability. In addition, different types of solutions were found, varying in all the parameters considered, (material, shape, thickness, and number of tanks), meaning that all of them can make a difference when selecting a specific design considering the demisability and the survivability.

Looking more closely at the resulting Pareto fronts, a first aspect is the difference in the output ranges for the two indices, with the demisability clearly having a wider range compared with the survivability. An important aspect also recognisable from the Pareto fronts is the importance of the mass of the satellite, especially for the demisability of a configuration. In particular, the interdependence between the mass of the satellite and the number of tanks in the assembly is very important. In fact, as the mass increases, only configurations with increasing number tanks produce fully demisable solutions. This also has an effect on the survivability because the *PNP* decreases with the increasing number of tanks. However, the gain in terms of demisability outweighs the survivability reduction as it is demonstrated by the optimiser always selecting the maximum number available of tanks for the most demisable solutions. Differently to the mission mass, the mission time does not influence the type of solutions in the Pareto front, but has the effect of shifting the solutions towards a lower survivability as the mission time increases. Finally, a comparison between three different demisability fitness functions has been carried out. All three functions have a common base that is represented by the Liquid Mass Fraction (Eq. 22), which is able to take into account the amount of mass demised through re-entry and the compliancy of a solution with the 15 J limit. However, Eq. 22 cannot differentiate between demisable solutions, as all designs with an impact energy below 15 J will be equal. That is why Eq. 24 was introduced, to take into account for the demisability altitude to differentiate between demisable solutions. This resulted (Figure 9) in solutions with an equivalent Pareto front except in the high demisability zones, where new solutions could be found. However, both the previous indices lacked the possibility of taking into account the negative effects of using increasing number of components. Eq. 22 and 24 are able to identify the good aspects of increasing the number of vessels, such as the increased demisability. However, if the solutions do not demise, having more components is negative as it results in an increased casualty area. Eq. 25 is actually able to take into account this behaviour, which results in Pareto fronts with penalised non-

demisable solutions, especially the one with higher number of surviving components.

ACKNOWLEDGMENTS

This work was funded by EPSRC DTP/CDT through the grant EP/K503150/1.

REFERENCES

1. B. O'Connor 2008. Handbook for Limiting Orbital Debris. NASA Handbook 8719.14. *National Aeronautics and Space Administration, Washington, DC*.
2. F. Schäfer, M. Lambert, E. Christiansen *et al.* The inter-agency space debris coordination committee (IADC) protection manual. 4th European Conference on Space Debris, 2005.
3. NASA 2012. Process for Limiting Orbital Debris. Washington, DC USA.
4. ESA 2008. Requirements on Space Debris Mitigation for ESA Projects.
5. R. L. Kelley 2012. Using the Design for Demise Philosophy to Reduce Casualty Risk Due to Reentering Spacecraft.
6. P. M. Waswa, and J. A. Hoffman 2012. Illustrative NASA Low Earth Orbit spacecraft subsystems design-for-demise trade-offs, analyses and limitations. *International Journal of Design Engineering,* 5**,** 21-40.
7. P. M. B. Waswa, M. Elliot, and J. A. Hoffman 2013. Spacecraft Design-for-Demise implementation strategy & decision-making methodology for low earth orbit missions. *Advances in Space Research,* 51**,** 1627-1637.
8. E. Christiansen 2009. Handbook for Designing MMOD Protection. Huston, Texas USA.
9. R. Putzar, and F. Schäfer, *Vulnerability of spacecraft equipment to space debris and meteoroids impacts,* Final Report, vol. 1, European Space Agency, 2006.
10. L. Grassi, F. Tiboldo, R. Destefanis *et al.* 2014. Satellite vulnerability to space debris – an improved 3D risk assessment methodology. *Acta Astronautica,* 99**,** 283-291.
11. M. Trisolini, H. G. Lewis, and C. Colombo. Survivability and Demise Criteria for Sustainable Spacecraft Design. 66th International Astronautical Conference, 2015 Jerusalem.
12. H. Schaub, L. E. Jasper, P. V. Anderson *et al.* 2015. Cost and risk assessment for spacecraft operation decisions caused by the space debris environment. *Acta Astronautica,* 113**,** 66-79.
13. M. Trisolini, H. G. Lewis, and C. Colombo, "Demise and Survivability Criteria for Spacecraft Design Optimisation," in International Association for the Avancement of Space Safety Conference, Melbourne, Florida, 2016.
14. NASA. 2009. *ORSAT* [Online]. NASA Orbital Debris Program Office. Available: http://orbitaldebris.jsc.nasa.gov/reentry/orsat.html [Accessed July 14 2015].
15. NASA. 2015. *Debris Assessment Software* [Online]. NASA Orbital Debris Program Office. Available: http://orbitaldebris.jsc.nasa.gov/mitigate/das.html [Accessed July 14 2015].
16. T. Lips, and B. Fritsche 2005. A comparison of commonly used re-entry analysis tools. *Acta Astronautica,* 57**,** 312-323.
17. E. Minisci 2015. Space Debris and Asteroids (Re)Entry Analysis Methods and Tools. Glasgow, UK: University of Strathclyde.
18. R. D. Klett, *Drag Coefficients and Heating Ratios for Right Circular Cylinder in Free-Molecular and Continuum Flow from Mach 10 to 30,* Technical Report SC-RR-64-2141, Sandia Report, SC-RR-64-2141, Albuquerque, 1964.
19. W. P. Hallman, and D. M. Moody, *Trajectory Reconstruction and Heating Analysis of Columbia Composite Debris Pieces*, The Aerospace Corporation, 2005.
20. T. M. Owens. 2014. *Aero-Thermal Demise of Reentry Debris: A Computational Model.* Master of Science, Florida Insititute of Technology.
21. J. Beck. May 5 2015. *RE: Personal Communication.*
22. J. Beck, J. Merrifield, I. Holbrough *et al.* 2015. Application of the SAM Destructive Re-Entry Code to the Spacecraft Demise Integration Test Cases. 8th European Symposium on Aerothermodynamics of Space Vehicles, March 2015 2015 Lisbon.
23. T. Lips, V. Wartemann, G. Koppenwallner *et al.* Comparison of ORSAT and SCARAB Reentry Survival Results. 4th European Conference on Space Debris, 18-20 April 2005 Darmstadt, Germany. 533.
24. NASA 1976. U.S. Standard Atmosphere 1976. Washington, D.C.
25. A. Tewari 2007. *Atmospheric and Space Flight Dynamics: Modeling and Simulation with MATLAB® and Simulink®*, Birkhäuser.
26. S. Flegel 2011. MASTER-2009 Software User Manual. Institute of Aerospace Systems (ILR).
27. N. Welty, M. Rudolph, F. Schäfer *et al.* 2013. Computational methodology to predict satellite system-level effects from impacts of untrackable space debris. *Acta Astronautica,* 88**,** 35-43.
28. K. Bunte, R. Destefanis, and G. Drolshagen. Spacecraft Shielding Layout and Optimisation Using ESABASE2/Debris. Proc. 5th European Conference on Space Debris, 2009.
29. A. Gäde, and A. Miller 2013. ESABASE2/Debris Release 6.0 Technical Description European Space Agency.
30. J. R. Wertz, and W. J. Larson 1999. *Space Mission*

Analysis and Design, Springer Netherlands.
31. S. Platnick. 2016. *NASA's Earth Observing System* [Online]. National Aeronautics and Space Administration. Available: http://eospso.nasa.gov/mission-category/3 [Accessed January 2016].
32. Airbus Safran Launchers GmbH. 2003. *Space Propulsion* [Online]. Bremen, Germany. Available: http://www.space-propulsion.com/index.html [Accessed July 2016].
33. European Space Agency. 2012. *Metop - meteorological missions* [Online]. European Space Agency. Available: http://www.esa.int/Our_Activities/Observing_the_Earth/The_Living_Planet_Programme/Meteorological_missions/MetOp/Overview14 [Accessed January 2016].
34. Airbus Safran Launchers GmbH. 2003. *20 N Chemical Monopropellant Hydrazine Thruster* [Online]. Airbus Safran Launchers GmbH,. Available: http://www.space-propulsion.com/spacecraft-propulsion/hydrazine-thrusters/20n-thruster.html 2017].
35. European Space Agency. 2016. *CryoSat-2 (Earth Explorer Opportunity Mission-2)* [Online]. eoPortal Directory. Available: https://eoportal.org/web/eoportal/satellite-missions/c-missions/cryosat-2 [Accessed July 2016].
36. K. Deb 2001. *Multi-objective optimization using evolutionary algorithms*, John Wiley & Sons.
37. K. Deb, A. Pratap, S. Agarwal *et al.* 2002. A fast and elitist multiobjective genetic algorithm: NSGA-II. *Evolutionary Computation, IEEE Transactions on,* 6**,** 182-197.
38. F. A. Fortin, F. M. De Rainville, M. A. Gardner *et al.* 2012. DEAP: Evolutionary Algorithms Made Easy. *Journal of Machine Learning Research,* 13**,** 2171-2175.
39. K. Deb, and R. B. Agrawal 1995. Simulated binary crossover for continuous search space. *Complex systems,* 9**,** 115-148.
40. K. Deb, and D. Deb 2014. Analysing mutation schemes for real-parameter genetic algorithms. *International Journal of Artificial Intelligence and Soft Computing,* 4**,** 1-28.
41. J. N. Opiela, E. Hillary, D. O. Whitlock *et al.*, *Debris Assessment Software Version 2.0 - User's Guide*, Lyndon B. Johnson Space Center, Huston, Texas, 2012.
42. ASM Aerospace Specification Metals Inc. 2016. *ASM Aerospace Specification Metals* [Online]. Pompano Beach, Florida. Available: http://www.aerospacemetals.com/contact-aerospace-metals.html [Accessed July 2016].
43. C. A. C. Coello 2002. Theoretical and numerical constraint-handling techniques used with evolutionary algorithms: a survey of the state of the art. *Computer methods in applied mechanics and engineering,* 191**,** 1245-1287.
44. B. Fritsche, T. Lips, and G. Koppenwallner 2007. Analytical and numerical re-entry analysis of simple-shaped objects. *Acta Astronautica,* 60**,** 737-751.